J. Fluid Mech. (1969), *vol.* 37, *part* 3, *pp.* 513–528
Printed in Great Britain

Initial propagation of impulsively generated converging cylindrical and spherical shock waves

By GLEN G. BACH AND JOHN H. LEE
Department of Mechanical Engineering, McGill University, Montreal

(Received 20 May 1968 and in revised form 29 October 1968)

An analytical description for the initial phases of collapse of a spherical or cylindrical shock wave in a perfect gas is given in the present paper. The shock wave is initiated by the instantaneous and uniform deposition of a finite quantity of energy per unit surface area at a finite radius R_0. For the initial shock motion where $x_s = (R_s - R_0)/R_0$ is small, analytical solutions are obtained by a power-series expansion of the dependent variables in x_s. The classical self-similar solution for a strong planar blast wave is recovered as the present zero-order solution. Non-similar effects arising from both finite shock strengths and the presence of a characteristic length R_0 are accounted for simultaneously in the present perturbation scheme. The analysis is carried out up to third order in x_s. For very large values of the initiation energy where the shock wave remains strong throughout its collapse, it is found that the present perturbation solution can adequately describe a significant portion of the collapse processes. The solution indicates that the shock decays rather rapidly initially and later begins to accelerate as a result of the additional adiabatic compression of the shocked states due to flow-area convergence. However, for weak initiation where the energy released is small, the present perturbation solution is an asymptotic series and diverges very rapidly as the shock propagates away from the wall. The range of validity then is limited to very small values of x_s.

1. Introduction

The motive for present analytical study of converging shock waves is the recent advances in quantitative experiments on implosion phenomena by Lee & Lee (1965) and Knystautas, Lee & Lee (1967). For converging shock waves generated initially at some finite radius R_0, there appears to be a lack of adequate analytical description of the implosion processes. For the final phases of the collapse, there exists the classical solution of Guderley (1942), Butler (1954) and Stanyukovich (1960). However, their self-similar solutions require the absence of a characteristic length and also that the shock front be of infinite strength (i.e. $M_s \to \infty$). Hence the similarity solution is applicable only in the immediate neighbourhood of the centre of convergence (i.e. $R_s/R_0 \to 0$), when both of these conditions can be realized in practice. Recently, attempts have been made by Lee (1966) and Welsh (1966) to extend the similarity solution to account for non-similar effects arising from finite shock strength. However, the validity of their

solutions is again confined to the vicinity of the centre of collapse since non-similar effects arising from the presence of a characteristic length R_0, R_s/R_0 being finite, was not accounted for in their analyses. The method of Chester (1954), Chisnell (1955) and Whitham (1958) for the propagation of shock waves in non-uniform channels has been found to yield fairly good predictions for the motion of the converging shock front itself. However, adequate description of the flow structure cannot be obtained by this method. It is also doubtful if the Chester–Chisnell–Whitham method can be used for describing the motion of converging shock waves under different initial conditions. For a complete description of the motion of imploding shock waves one must resort to a number of numerical schemes whereby the conservation equations of motion can be integrated numerically (Payne 1957 and Brode 1955). These numerical schemes are extremely time consuming and are used only for particular cases of interest.

The aim of the present work is to provide an analytical description for the initial phases of collapse of spherical and cylindrical shock waves generated in a chamber of finite size. The model assumes a shock wave to be initiated by the instantaneous and uniform deposition of finite quantity of energy per unit surface area of a spherical or cylindrical shell. Such a model simulates the experimental condition of initiation by the detonation of a thin spherical or cylindrical sheet of high explosives (Glass 1965), or by the electrical explosion of a cylindrical foil (Dennen & Wilson 1962). The propagation of converging shock waves generated by other means such as arbitrary piston motion, will be considered in a subsequent paper.

2. Formulation

Consider a spherical or cylindrical chamber of radius R_0 containing a test gas at initial pressure p_0 and initial density ρ_0. At time $t = 0$ a finite quantity of energy E_0 or, for the cylindrical case E_0 per unit length is released instantaneously at R_0, generating a strong shock wave. At subsequent times, the shock wave collapses toward the centre or the axis of symmetry.

Neglecting viscous and heat transfer effects, and assuming a perfect gas with constant specific-heat ratio γ, the conservation equations governing the adiabatic motion of the shocked gas can be written as follows:

conservation of mass

$$\frac{\partial \rho}{\partial t} + \frac{\partial (\rho u)}{\partial r} + j\frac{\rho u}{r} = 0, \tag{2.1}$$

conservation of momentum

$$\frac{\partial u}{\partial t} + u\frac{\partial u}{\partial r} + \frac{1}{\rho}\frac{\partial p}{\partial r} = 0, \tag{2.2}$$

conservation of energy

$$\left(\frac{\partial}{\partial t} + u\frac{\partial}{\partial r}\right)\frac{p}{\rho^\gamma} = 0, \tag{2.3}$$

where $j = 1$ for cylindrical symmetry,

$= 2$ for spherical symmetry.

The boundary conditions at the shock front $r = R_s$ are given by the standard Rankine–Hugoniot relationships for a normal shock in a perfect gas as follows:

$$\frac{\rho_1}{\rho_0} = \frac{\gamma+1}{\gamma-1+2/M_s^2}, \tag{2.4}$$

$$\frac{u_1}{\dot{R}_s} = \frac{2}{\gamma+1}\left(1-\frac{1}{M_s^2}\right), \tag{2.5}$$

$$\frac{p_1}{\rho_0 \dot{R}_s^2} = \frac{2}{\gamma+1} - \frac{\gamma-1}{\gamma(\gamma+1)}\frac{1}{M_s^2}, \tag{2.6}$$

where M_s is the shock Mach number defined as

$$M_s = |\dot{R}_s|/c_0 = |\dot{R}_s|/\sqrt{(\gamma p_0/\rho_0)}. \tag{2.7}$$

The subscript 1 denotes conditions immediately behind the shock front while $\dot{R}_s$ and c_0 are the shock velocity and the sound speed of the undisturbed medium, respectively. In the present problem, it is more convenient to use a set of non-dimensional variables similar to that used in blast-wave studies, Rae & Kirchner (1963). The variables are given by

$$\phi(\xi, x_s) = u(r,t)/\dot{X}_s(t), \tag{2.8}$$

$$f(\xi, x_s) = p(r,t)/\rho_0 \dot{X}_s^2(t), \tag{2.9}$$

$$\psi(\xi, x_s) = \rho(r,t)/\rho_0, \tag{2.10}$$

where

$$\xi = (r-R_0)/(R_s-R_0), \tag{2.11}$$

$$X_s = R_s - R_0, \tag{2.12}$$

and

$$x_s = X_s/R_0 = (R_s-R_0)/R_0. \tag{2.13}$$

Equations (2.1)–(2.3) transform to the following equations, respectively.

$$(\phi-\xi)\frac{\partial \psi}{\partial \xi} + \psi\frac{\partial \phi}{\partial \xi} + j\frac{\phi\psi x_s}{1+x_s\xi} = -x_s\frac{\partial \psi}{\partial x_s}, \tag{2.14}$$

$$(\phi-\xi)\frac{\partial \phi}{\partial \xi} + \theta\phi + \frac{1}{\psi}\frac{\partial f}{\partial \xi} = -x_s\frac{\partial \phi}{\partial x_s}, \tag{2.15}$$

$$(\phi-\xi)\left(\frac{\partial f}{\partial \xi} - \frac{\gamma f}{\psi}\frac{\partial \psi}{\partial \xi}\right) + 2\theta f = -x_s\left(\frac{\partial f}{\partial x_s} - \frac{\gamma f}{\psi}\frac{\partial \psi}{\partial x_s}\right), \tag{2.16}$$

where the parameter θ is defined as

$$\theta = x_s\ddot{x}_s/\dot{x}_s^2, \tag{2.17}$$

and $\dot{x}_s$, $\ddot{x}_s$ denote first and second derivatives of x_s with respect to time t. A more convenient form of the energy equation can be obtained by eliminating ψ from equations (2.14) and (2.16). Re-arranging the resultant equation one obtains

$$(\phi-\xi)\frac{\partial f}{\partial \xi} + \gamma f\frac{\partial \phi}{\partial \xi} + 2\theta f + j\frac{\gamma f\phi x_s}{1+x_s\xi} = -x_s\frac{\partial f}{\partial x_s}. \tag{2.18}$$

The region of flow governed by equations (2.14)–(2.18) is bounded by the shock front of $\xi = 1$ and by the chamber wall at $\xi = 0$. The shock originates at the chamber wall $x_s = 0$ and collapses to the centre at $x_s = -1$.

In contrast to the classical solution for the final phases of collapse, the energy integral provides a useful relationship in the present problem since the flow boundaries are finite (i.e. $1 \geqslant \xi \geqslant 0$). Conservation of the total energy at any instant of time yields the relationship

$$E_0 = \int_{R_s}^{R_0} \left(\frac{p}{\gamma-1} + \tfrac{1}{2}\rho u^2\right) k_j r^j \, dr - \int_{R_s}^{R_0} \frac{p_0}{\gamma-1} k_j r^j \, dr, \tag{2.19}$$

where the numerical constant k_j is defined as

$$k_1 = 2\pi \text{ for } j = 1 \quad \text{(cylindrical symmetry)},$$
$$k_2 = 4\pi \text{ for } j = 2 \quad \text{(spherical symmetry)}.$$

The second integral on the right-hand side of equation (2.19) represents the initial internal energy of the medium. Evaluating this integral and expressing the resultant equation in terms of the previously defined dimensionless variables, one obtains

$$E_0 = \rho_0 k_j R_0^{j+3} \dot{x}_s^2 x_s [I(x_s) - c_0^2\{1-(1+x_s)^{j+1}\}/\{\gamma(\gamma-1)(j+1)x_s\dot{x}_s^2\}], \tag{2.20}$$

where

$$I(x_s) = \int_1^0 \left(\frac{f}{\gamma-1} + \tfrac{1}{2}\psi\phi^2\right)(1+x_s\xi)^j \, d\xi. \tag{2.21}$$

If the intiation energy E_0 is large compared to the initial internal energy of the medium, the second term on the right-hand side of equation (2.20) can be neglected. However, in contrast to the classical strong blast wave problem similarity solutions cannot be obtained here even under this condition. The presence of the characteristic length R_0 results in the integral $I(x_s)$ being dependent on the shock position x_s. From equation (2.20), it is seen that in the present problem, departure from similarity arises from both time-dependent boundary conditions when the initial internal energy of the medium cannot be neglected as compared to E_0, and also from the presence of a characteristic length R_0.

In the subsequent analysis, it is more convenient to seek an appropriate characteristic time so that the time variable t can be made non-dimensional, and this characteristic time t_j^* is defined by

$$t_j^* = \sqrt{\left(\frac{\rho_0 k_j R_0^{j+3}}{(j+1)E_0}\right)}. \tag{2.22}$$

t_j^* can be interpreted as the order of magnitude of the total time of collapse.

In the subsequent analysis, the non-dimensional time variable τ, where

$$\tau = t/t_j^* \tag{2.23}$$

will be used. The shock velocity $\dot{R}_s$ or $\dot{X}_s$ now becomes

$$\dot{R}_s = \dot{X}_s = R_0\dot{x}_s = \frac{R_0}{t_j^*}\frac{dx_s}{d\tau}.$$

Equations (2.14)–(2.18) remain unchanged except that $\dot{x}_s$ now represents differentiation with respect to τ. The energy integral (i.e. equation (2.20)) can be rewritten as

$$1 = x_s\dot{x}_s^2(j+1)I(x_s) - c_j^{*2}\{1-(1+x_s)^{j+1}\}/\{\gamma(\gamma-1)\}, \tag{2.24}$$

where c_j^* is the characteristic sound speed defined as

$$c_j^{*2} = c_0^2 t_j^{*2}/R_0^2. \tag{2.25}$$

If the initiation energy is very large (i.e. $E_0 \to \infty$), then $t_j^* \to 0$, $c_j^{*2} \to 0$ and the shock wave remains strong throughout its collapse. For example, in a spherical implosion chamber of radius 3 cm containing air at 10 mm Hg initial pressure, an initiation energy of 10 joules gives a value of $t_2^* = 12{\cdot}5 \times 10^{-6}$ sec and $c_2^{*2} = 0{\cdot}0196$. For hydrogen under identical conditions, $t_2^* = 0{\cdot}346 \times 10^{-6}$ sec, while $c_2^{*2} = 0{\cdot}0199$, approximately the same as that for air due to the higher sound speed in hydrogen.

3. Analysis

For the initial phases of the collapse when $|x_s| \ll 1$, one may seek solutions to equations (2.14) to (2.18) by assuming the following power series for the dependent variables ϕ, f and ψ.

$$\left.\begin{aligned} \phi(\xi, x_s) &= \sum_{n=0}^{\infty} \phi^{(n)}(\xi)\, x_s^n, \\ f(\xi, x_s) &= \sum_{n=0}^{\infty} f^{(n)}(\xi)\, x_s^n, \\ \psi(\xi, x_s) &= \sum_{n=0}^{\infty} \psi^{(n)}(\xi)\, x_s^n. \end{aligned}\right\} \tag{3.1}$$

An appropriate expansion for the shock velocity $\dot{x}_s$ can readily be obtained by inspection from the energy integral given by equation (2.24). Since the left-hand side of equation (2.24) is finite, $\dot{x}_s^2$ must be of the form

$$\dot{x}_s^2 = \frac{1}{x_s} \sum_{n=0}^{\infty} F_n x_s^n. \tag{3.2}$$

From equation (3.2), one can readily determine the expansion for the parameter θ as

$$\theta(x_s) = \sum_{n=0}^{\infty} \theta^{(n)} x_s^n, \tag{3.3}$$

where the coefficients $\theta^{(0)}, \theta^{(1)}, \theta^{(2)}, \ldots$ are given by

$$\theta^{(0)} = -\tfrac{1}{2},\ \theta^{(1)} = \tfrac{1}{2}F_1/F_0, \tag{3.4}$$

$$\theta^{(2)} = F_2/F_0 - \tfrac{1}{2}F_1^2/F_0^2, \tag{3.5}$$

$$\theta^{(3)} = \tfrac{1}{2}\{(F_1/F_0)^3 - 3F_1F_2/F_0^2 + 3F_3/F_0\}, \tag{3.6}$$

Substituting the perturbation expressions given by equations (3.1)–(3.6) into the conservation equations (equations (2.14), (2.15) and (2.18)) and into the energy integral (equation (24.4)), one obtains the following after equating coefficients of similar orders in x_s.

Zeroth order:

$$(\phi^{(0)} - \xi)\,\psi^{(0)\prime} + \psi^{(0)}\phi^{(0)\prime} = 0, \tag{3.7}$$

$$(\phi^{(0)} - \xi)\,\phi^{(0)\prime} + f^{(0)\prime}/\psi^{(0)} = -\theta^{(0)}\phi^{(0)}, \tag{3.8}$$

$$(\phi^{(0)}-\xi)\,f^{(0)\prime}+\gamma f^{(0)}\phi^{(0)\prime} = -2\theta^{(0)}f^{(0)}, \tag{3.9}$$

$$F_0 = 1/\{(j+1)\,I^{(0)}\}, \tag{3.10}$$

where

$$I_0 = \int_1^0 d\xi\{f^{(0)}/(\gamma-1)+\tfrac{1}{2}\phi^{(0)2}\psi^{(0)}\}. \tag{3.11}$$

First order

$$(\phi^{(0)}-\xi)\,\psi^{(1)\prime}+\psi^{(0)}\phi^{(1)\prime} = -\{\psi^{(1)}(\phi^{(0)\prime}+1)+\phi^{(1)}\psi^{(0)\prime}+j\phi^{(0)}\psi^{(0)}\}, \tag{3.12}$$

$$(\phi^{(0)}-\xi)\,\phi^{(1)\prime}+f^{(1)\prime}/\psi^{(0)} = -\{\phi^{(1)}(\phi^{(0)\prime}+1+\theta^{(0)})+\theta^{(1)}\phi^{(0)}-\psi^{(1)}f^{(0)\prime}/\psi^{(0)2}\}, \tag{3.13}$$

$$(\phi^{(0)}-\xi)\,f^{(1)\prime}+\gamma f^{(0)}\phi^{(1)\prime} = -\{f^{(1)}(\gamma\phi^{(0)\prime}+1+2\theta^{(0)})+2\theta^{(1)}f^{(0)}+\phi^{(1)}f^{(0)\prime}+j\gamma f^{(0)}\phi^{(0)}\}, \tag{3.14}$$

$$F_1 = -(c_j^{*2}/\{\gamma(\gamma-1)\}+F_0 I^{(1)})/I^{(0)}, \tag{3.15}$$

where

$$I^{(1)} = \int_1^0 d\xi\,[j\xi\{f^{(0)}/(\gamma-1)+\tfrac{1}{2}\phi^{(0)2}\psi^{(0)}\}+f^{(1)}/(\gamma-1)+\tfrac{1}{2}\phi^{(0)2}\psi^{(1)}+\phi^{(0)}\phi^{(1)}\psi^{(0)}]. \tag{3.16}$$

Second order:

$$\begin{aligned}(\phi^{(0)}-\xi)\,\psi^{(2)\prime}+\psi^{(0)}\phi^{(2)\prime} = &-\{\psi^{(2)}(\phi^{(0)\prime}+2)+\psi^{(1)}\phi^{(1)\prime}+\phi^{(2)}\psi^{(0)\prime}\\ &+\phi^{(1)}\psi^{(1)\prime}-j\xi\phi^{(0)}\psi^{(0)}+j(\phi^{(0)}\psi^{(1)}+\phi^{(1)}\psi^{(0)})\},\end{aligned} \tag{3.17}$$

$$\begin{aligned}(\phi^{(0)}-\xi)\,\phi^{(2)\prime}+f^{(2)\prime}/\psi^{(0)} = &-\{\phi^{(2)}(\phi^{(0)\prime}+\theta^{(0)}+2)+\phi^{(1)}(\phi^{(1)\prime}+\theta^{(1)})\\ &+\phi^{(0)}\theta^{(2)}-\psi^{(1)}f^{(1)\prime}/\psi^{(0)2}+(\psi^{(1)2}/\psi^{(0)}-\psi^{(2)})\,f^{(0)\prime}/\psi^{(0)2}\},\end{aligned} \tag{3.18}$$

$$\begin{aligned}(\phi^{(0)}-\xi)\,f^{(2)\prime}+\gamma f^{(0)}\phi^{(2)\prime} = &-\{f^{(2)}(\gamma\phi^{(0)\prime}+2\theta^{(0)}+2)+f^{(1)}(\gamma\phi^{(1)\prime}+2\theta^{(1)})+2\theta^{(2)}f^{(0)}\\ &+\phi^{(2)}f^{(0)\prime}+\phi^{(1)}f^{(1)\prime}-j\gamma\xi\phi^{(0)}f^{(0)}+j\gamma(\phi^{(0)}f^{(1)}+\phi^{(1)}f^{(0)})\},\end{aligned} \tag{3.19}$$

$$F_2 = -[jc_j^{*2}/\{2\gamma(\gamma-1)\}+F_1 I^{(1)}+F_0 I^{(2)}]/I^{(0)}, \tag{3.20}$$

where

$$\begin{aligned}I^{(2)} = \int_1^0 d\xi\,[&f^{(2)}/(\gamma-1)+\tfrac{1}{2}\psi^{(2)}\phi^{(0)2}+\tfrac{1}{2}\psi^{(0)}\phi^{(1)2}+\psi^{(0)}\phi^{(0)}\phi^{(2)}+\psi^{(1)}\phi^{(1)}\phi^{(0)}\\ &+j\xi\{f^{(1)}/(\gamma-1)+\tfrac{1}{2}\psi^{(1)}\phi^{(0)2}+\psi^{(0)}\phi^{(0)}\phi^{(1)}\}+\tfrac{1}{2}j(j-1)\,\xi^2\{f^{(0)}/(\gamma-1)+\tfrac{1}{2}\psi^{(0)}\phi^{(0)2}\}].\end{aligned} \tag{3.21}$$

Third order:

$$\begin{aligned}(\phi^{(0)}-\xi)\,\psi^{(3)\prime}+\psi^{(0)}\phi^{(3)\prime} = &-\{\psi^{(3)}(\phi^{(0)\prime}+3)+\psi^{(2)}\phi^{(1)\prime}+\psi^{(1)}\phi^{(2)\prime}\\ &+\phi^{(3)}\psi^{(0)\prime}+\phi^{(2)}\psi^{(1)\prime}+\phi^{(1)}\psi^{(2)\prime}+j(\phi^{(0)}\psi^{(2)}+\phi^{(1)}\psi^{(1)}+\phi^{(2)}\psi^{(0)})\\ &-j\xi(\phi^{(0)}\psi^{(1)}+\phi^{(1)}\psi^{(0)})+j\xi^2\phi^{(0)}\psi^{(0)}\},\end{aligned} \tag{3.22}$$

$$\begin{aligned}(\phi^{(0)}-\xi)\,\phi^{(3)\prime}+f^{(3)\prime}/\psi^{(0)} = &-\{\phi^{(3)}(\phi^{(0)\prime}+\theta^{(0)}+3)+\phi^{(2)}(\phi^{(1)\prime}+\theta^{(1)})\\ &+\phi^{(1)}(\phi^{(2)\prime}+\theta^{(2)})+\phi^{(0)}\theta^{(3)}-\psi^{(1)}f^{(2)\prime}/\psi^{(0)2}+(\psi^{(1)2}/\psi^{(0)}-\psi^{(2)})\,f^{(1)\prime}/\psi^{(0)2}\\ &-(\psi^{(1)3}/\psi^{(0)2}-2\psi^{(1)}\psi^{(2)}/\psi^{(0)}+\psi^{(3)})\,f^{(0)\prime}/\psi^{(0)2}\},\end{aligned} \tag{3.23}$$

$$\begin{aligned}(\phi^{(0)}-\xi)\,f^{(3)\prime}+\gamma f^{(0)}\phi^{(3)\prime} = &-\{f^{(3)}(\gamma\phi^{(0)\prime}+2\theta^{(0)}+3)+f^{(2)}(\gamma\phi^{(1)\prime}+2\theta^{(1)})\\ &+f^{(1)}(\gamma\phi^{(2)\prime}+2\theta^{(2)})+2\theta^{(3)}f^{(0)}+\phi^{(3)}f^{(0)\prime}+\phi^{(2)}f^{(1)\prime}+\phi^{(1)}f^{(2)\prime}+j\gamma\xi^2\phi^{(0)}f^{(0)}\\ &-j\gamma\xi(\phi^{(0)}f^{(1)}+\phi^{(1)}f^{(0)})+j\gamma(\phi^{(0)}f^{(2)}+\phi^{(1)}f^{(1)}+\phi^{(2)}f^{(0)})\},\end{aligned} \tag{3.24}$$

$$F_3 = -\{j(j-1)c_j^{*2}/(6\gamma(\gamma-1))+F_0 I^{(3)}+F_1 I^{(2)}+F_2 I^{(1)}\}/I^{(0)}, \tag{3.25}$$

where

$$I^{(3)} = \int_1^0 d\xi[f^{(3)}/(\gamma-1) + \tfrac{1}{2}\psi^{(3)}\phi^{(0)2} + \tfrac{1}{2}\psi^{(1)}\phi^{(1)2} + \psi^{(0)}\phi^{(0)}\phi^{(3)} + \psi^{(0)}\phi^{(1)}\phi^{(2)}$$
$$+ \psi^{(1)}\phi^{(0)}\phi^{(2)} + \psi^{(2)}\phi^{(0)}\phi^{(1)} + j\xi\{f^{(2)}/(\gamma-1) + \tfrac{1}{2}\psi^{(2)}\phi^{(0)2} + \tfrac{1}{2}\psi^{(0)}\phi^{(1)2}$$
$$+ \psi^{(0)}\phi^{(0)}\phi^{(2)} + \psi^{(1)}\phi^{(1)}\phi^{(0)}\} + \tfrac{1}{2}j(j-1)\,\xi^2\{f^{(1)}/(\gamma-1) + \tfrac{1}{2}\psi^{(1)}\phi^{(0)2} + \psi^{(0)}\phi^{(0)}\phi^{(1)}\}] \tag{3.26}$$

The boundary conditions to be satisfied by the zeroth-, first-, second- and third-order equations at the shock front $\xi = 1$ can be determined by expanding the Rankine–Hugoniot relations. Substituting equation (3.2) into equations (2.4)–(2.6) and carrying out the expansions, one obtains for

Zeroth order:

$$\phi^{(0)}(1) = f^{(0)}(1) = 2/(\gamma+1), \tag{3.27}$$
$$\psi^{(0)}(1) = (\gamma+1)/(\gamma-1). \tag{3.28}$$

First order:

$$\psi^{(1)}(1) = -2c_j^{*2}(\gamma+1)/\{F_0(\gamma-1)^2\}, \tag{3.29}$$
$$\phi^{(1)}(1) = -2c_j^{*2}/\{F_0(\gamma+1)\}, \tag{3.30}$$
$$f^{(1)}(1) = \tfrac{1}{2}(\gamma-1)\phi^{(1)}(1)/\gamma. \tag{3.31}$$

Second order:

$$\psi^{(2)}(1) = 2c_j^{*2}(\gamma+1)/\{(\gamma-1)^2F_0^2\}(F_1 + 2c_j^{*2}/\gamma - 1), \tag{3.32}$$
$$\phi^{(2)}(1) = 2c_j^{*2}F_1/\{(\gamma+1)F_0^2\}, \tag{3.33}$$
$$f^{(2)}(1) = \tfrac{1}{2}(\gamma-1)\phi^{(2)}(1)/\gamma. \tag{3.34}$$

Third order:

$$\psi^{(3)}(1) = -2c_j^{*2}(\gamma+1)/\{(\gamma-1)^2F_0^3\}\,[\{F_1 + 2c_j^{*2}/(\gamma-1)\}^2 - F_0F_2], \tag{3.35}$$
$$\phi^{(3)}(1) = -2c_j^{*2}/\{(\gamma+1)F_0^3\}\,(F_1^2 - F_0F_2), \tag{3.36}$$
$$f^{(3)}(1) = \tfrac{1}{2}(\gamma-1)\,\phi^{(3)}(1)/\gamma. \tag{3.37}$$

The zeroth-order shock boundary conditions are simply those for an infinitely strong shock wave of limiting density ratio. The parameter c_j^{*2} appears in the first- and higher-order boundary conditions only. Hence for very large values of the initiation energy E_0 where c_j^{*2} can be neglected, the first- and higher-order boundary conditions all become zero. The shock remains strong throughout its collapse under this condition. One should note that the determination of the boundary conditions for a higher-order solution requires the complete solution of the lower-order equations. For example, the first-order boundary conditions can only be evaluated after the zeroth-order solution is obtained and F_0 determined from the zeroth-order energy integral (i.e. equation (3.10)).

From the differential equations for the zeroth-order (i.e. equations (3.7)–(3.9)), its boundary conditions (i.e. equations (3.27) and (3.28)), and the value of $\theta^{(0)} = -\frac{1}{2}$, one observes immediately that the solution will in fact be the

self-similar solution for strong planar blast waves. One would expect this result since the shock is initiated at the wall surface at R_0 and for very short times after initiation, curvature effects are negligible and the flow is essentially planar.

With the zeroth-order solution known, F_0 can be evaluated from the energy integral (i.e. equation (3.10)), and the first-order boundary conditions can now be determined. With these as starting values at the shock $\xi = 1$, the differential equations for the first-order (i.e. equations (3.12)–(3.14)) can then be integrated numerically with a chosen value of $\theta^{(1)}$. The criterion for determining the correct solution will be when the chosen value of $\theta^{(1)}$ gives a solution that satisfies the condition of zero particle velocity at the wall. An alternative criterion will be when the assumed value of $\theta^{(1)}$ coincides with the value obtained from the first-order energy integral. In the present study, rapid convergence is obtained using the *regula-falsi* method of iteration for $\theta^{(1)}$ based on the criterion of zero particle velocity at the wall ($\xi = 0$, $\phi^{(1)}(0) = 0$). The second criterion is also used to check the value of the $\theta^{(1)}$ obtained. The solutions for the second- and higher-orders are found in a similar manner.

The shock trajectory can be obtained from the definition of the shock velocity

$$\dot{x}_s = dx_s/d\tau,$$

or

$$\tau = \int_0^{x_s} dx_s/\dot{x}_s. \tag{3.38}$$

Substituting the expansion for $\dot{x}_s^2$ in terms of x_s into the above equation, one obtains

$$\tau = -\int_0^{x_s} dx_s \sqrt{\{(F_0/x_s + F_1 + F_2 x_s + F_3 x_s^2 + \ldots)\}^{-1}}, \tag{3.39}$$

where the negative square root of $\dot{x}_s^2$ is taken since the shock velocity is directed towards the centre of symmetry.

Integrating equation (3.38) up to third order in x_s, the resultant expression for the shock trajectory becomes

$$\tau = B_0 |x_s|^{\frac{3}{2}} (1 + B_1 x_s + B_2 x_s^2 + B_3 x_s^3 + \ldots), \tag{3.40}$$

where

$$B_0 = 2\{3\sqrt{|F|}\}_0,$$

$$B_1 = -\tfrac{3}{10} F_1/F_0,$$

$$B_2 = \tfrac{3}{7}(\tfrac{3}{8} F_1^2/F_0^2 - \tfrac{1}{2} F_2/F_0),$$

$$B_3 = -\tfrac{1}{3}(\tfrac{5}{16}(F_1/F_0)^3 - \tfrac{3}{4} F_1 F_2/F_0^2 + \tfrac{1}{2} F_3/F_0).$$

4. Results

For the results presented in this paper, a value of γ is 1·4 for both the spherical and the cylindrical cases only. The planar case $j = 0$ is not of interest since no area convergence and shock amplification exist and it is simply the ordinary planar blast problem.

From equations (3.27) to (3.37) one notes that the nth-order boundary conditions are of the form of an nth-order polynomial in the parameter c_j^{*2}. Hence the

perturbation coefficients (i.e. F_n, $\theta^{(n)}$, $I^{(n)}$, B_n, etc.) can be written in the following form:

$$\chi_n = \chi_{n0} + \chi_{n1} c_j^{*2} + \chi_{n2} c_j^{*4} + \ldots = \sum_{i=0}^{n} \chi_{ni} c_j^{*2i}, \tag{4.1}$$

where χ denotes any one of the perturbation coefficients. Numerical results for the χ_n are given in table 1 for the spherical case and table 2 for the cylindrical case. For example, from table 1 the parameter θ can be written as

$$\begin{aligned}\theta = & -0{\cdot}5 + x_s(-0{\cdot}61284 - 3{\cdot}8972 c_j^{*2}) \\ & + x_s^2(0{\cdot}50016 - 7{\cdot}64711 c_j^{*2} - 48{\cdot}368 c_j^{*4}) \\ & + x_s^3(-0{\cdot}46982 - 2{\cdot}6796 c_j^{*2} - 131{\cdot}74 c_j^{*4} - 687{\cdot}39 c_j^{*6}) + \ldots .\end{aligned} \tag{4.2}$$

		$i=0$	$i=1$	$i=2$	$i=3$
$\chi = F$	F_{0i}	−0·27499	—	—	—
	F_{1i}	0·33705	2·14334	—	—
	F_{2i}	−0·34409	−0·52417	4·94771	—
	F_{3i}	0·33910	0·59577	1·69620	44·0491
$\chi = \theta$	$\theta_i^{(0)}$	−0·5	—	—	—
	$\theta_i^{(1)}$	−0·61284	−3·89715	—	—
	$\theta_i^{(2)}$	0·50016	−7·64711	−48·3680	—
	$\theta_i^{(3)}$	−0·46982	−2·67964	−131·7374	−687·3912
$\chi = B$	B_{0i}	1·27131	—	—	—
	B_{1i}	0·36770	2·33829	—	—
	B_{2i}	−0·026698	2·66223	13·61909	—
	B_{3i}	0·013903	0·99789	26·09604	111·0813
$\chi = I$	$I_i^{(0)}$	−1·21217	—	—	—
	$I_i^{(1)}$	−1·48573	−2·95425	—	—
	$I_i^{(2)}$	−0·30423	−6·39679	−44·8362	—
	$I_i^{(3)}$	−0·008565	−3·01314	−133·3906	−596·793

TABLE 1. Perturbation coefficients for a spherical implosion

		$i=0$	$i=1$	$i=2$	$i=3$
$\chi = F$	F_{0i}	−0·41248	—	—	—
	F_{1i}	0·25278	2·14334	—	—
	F_{2i}	−0·18423	−0·26209	3·29847	—
	F_{3i}	0·14780	0·24607	0·56540	19·5774
$\chi = \theta$	$\theta_i^{(0)}$	−0·5	—	—	—
	$\theta_i^{(1)}$	−0·30642	−2·59810	—	—
	$\theta_i^{(2)}$	0·25886	−2·54904	−21·4969	—
	$\theta_i^{(3)}$	−0·24195	0·24325	−29·2750	−203·671
$\chi = B$	B_{0i}	1·03802	—	—	—
	B_{1i}	0·18385	1·55886	—	—
	B_{2i}	−0·03535	0·88741	6·05293	—
	B_{3i}	0·01526	0·031717	5·79912	32·9130
$\chi = I$	$I_i^{(0)}$	−1·21217	—	—	—
	$I_i^{(1)}$	−0·74286	−1·96950	—	—
	$I_i^{(2)}$	0·08616	−2·13226	−19·9272	—
	$I_i^{(3)}$	−0·04972	0·05831	−29·6423	−176·827

TABLE 2. Perturbation coefficients for a cylindrical implosion

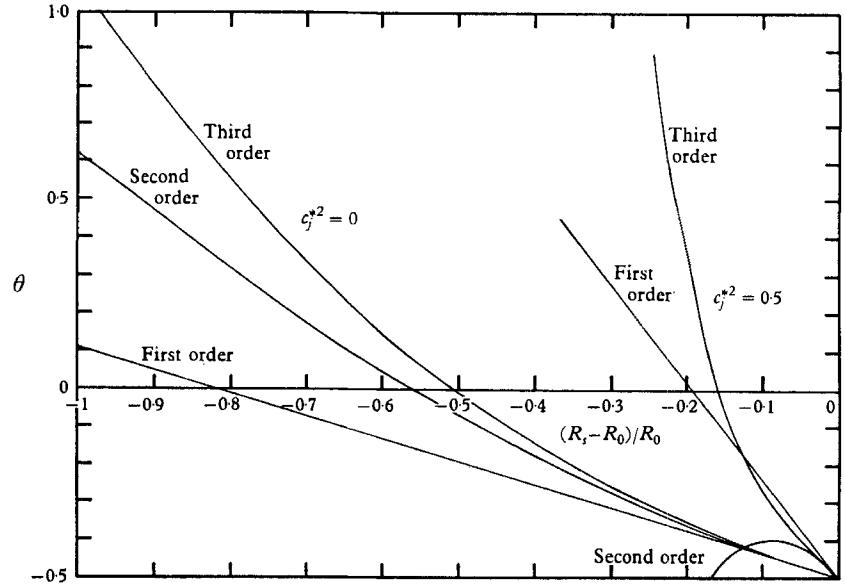

FIGURE 1. Shock decay coefficient for varying initiation energy (spherical implosion).

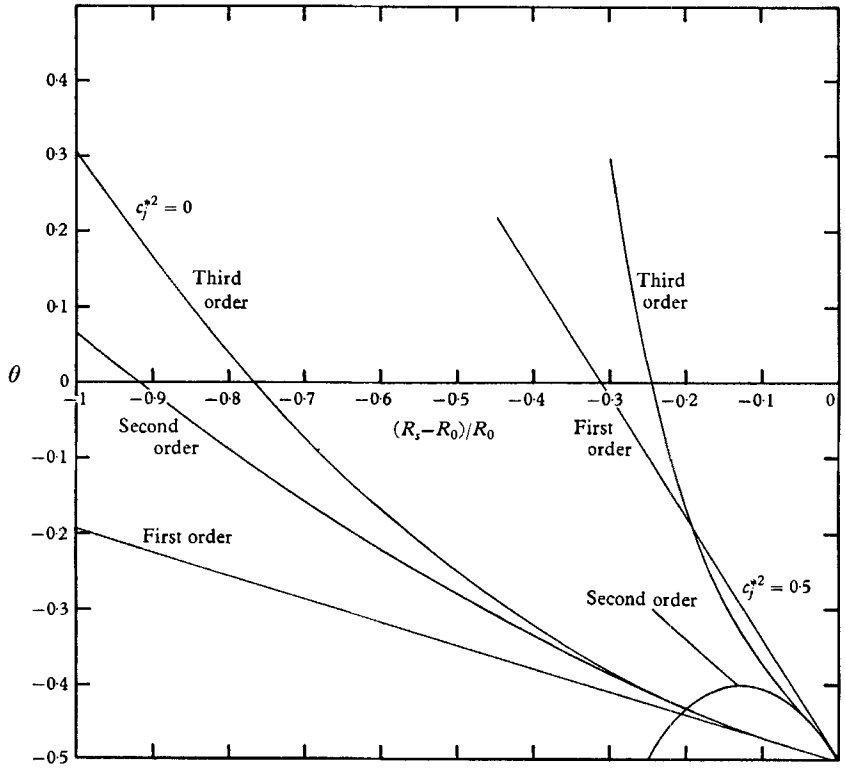

FIGURE 2. Shock decay coefficient for varying initiation energy (cylindrical implosion).

From tables 1 and 2 one notes that for $c_j^{*2} = 0$, all the higher-order corrections have the same sign since x_s is negative, which indicates that for very large initiation energy the present perturbation expansion are simple Taylor series about the wall $x_s = 0$. However, for finite values of c_j^{*2}, the higher-order perturbation coefficients have alternating signs and increasing magnitudes, which are characteristics of an asymptotic type of expansion similar to the solution of Sakurai (1954) for blast waves with counter-pressure effects.

The variation of θ with the shock location x_s for the spherical and cylindrical cases are shown in figures 1 and 2, respectively, for two values of c_j^{*2} ($c_j^{*2} = 0$ and 0·5). Also plotted in these figures are the corrections for the different orders to indicate the region of validity and the accuracy of the present third-order solution. The asymptotic nature of the solution for finite values of c_j^{*2} is clearly demonstrated by the set of curves for $c_j^{*2} = 0{\cdot}5$. For $c_j^{*2} = 0{\cdot}0$, one notes that the present third-order solution yields a fairly good description of the implosion processes for more than 50 % of the shock travel. From the definition of the parameter θ (i.e. equation (2.17)), it can be seen that its sign, positive or negative, denotes whether the shock is accelerating or decelerating, respectively. Figures 1 and 2 indicate that the shock initially decelerates as the initiation energy is being distributed over an increasing mass of gas engulfed by the shock. However, as the shock collapses to smaller radii, the amplification mechanism of flow convergence begins to play an increasingly important role and the shock accelerates. Comparing figures 1 and 2, one notes that the amplification mechanism is stronger for the spherical case than for the cylindrical case. For the spherical case, θ changes sign at about 50 % of the shock travel while in the cylindrical case the shock only begins to accelerate after about 75 % of its total travel.

The present solution, even for $c_j^{*2} = 0$, is not valid in the vicinity of the centre of convergence, i.e. $x_s \to -1{\cdot}0$. From the asymptotic solution of Guderley (1942) one notes that $R_s\ddot{R}_s/\dot{R}_s^2 \to$ a finite negative number as $R_s \to 0$. In the present analysis θ can be written as

$$\theta = \frac{x_s}{1+x_s}\frac{R_s\ddot{R}_s}{\dot{R}_s^2}. \tag{4.3}$$

From the above equation one notes that $\theta \to +\infty$ as $x_s \to -1$.

The shock trajectories for a range of c_j^{*2} for the spherical case are shown in figure 3. For $c_j^{*2} = 0$, which corresponds to an infinitely strong collapsing shock wave, one notes from the relative magnitude of the higher-order corrections that the present third-order solution probably gives a fairly accurate description of the shock motion for the majority of its collapse. A change in curvature of the shock trajectory can be observed, and the location of the point of inflexion corresponds to the same shock position when $\theta = 0$ in figure 1. For finite values of c_j^{*2}, the range of validity of the present third-order trajectories decreases. All trajectories coalesce near the wall ($x_s = 0$) since the shock is strong initially (i.e. $M_s^2 \to \infty$), and flow-convergence effects are small at large shock radii for all radius of c_j^{*2}. The shock motion is then identical to a strong planar blast wave (i.e. $R_s \sim t^{\frac{2}{3}}$).

A comparison of the shock trajectories for strong planar, cylindrical and spherical implosions (i.e. $c_j^{*2} = 0$) is illustrated in figure 4. To obtain a proper

time scale for the comparison, the characteristic time t_j^*, function of the geometry j, must be referenced to that of the planar case (i.e. t_0^*) in order to have the same initiation energy density per unit area for all the three cases. From equation (2.22) one notes that for the same energy density, $t_2^*/t_0^* = 1/\sqrt{3}$ and $t_1^*/t_0^* = 1/\sqrt{2}$. In figure 4 the planar-blast trajectory is simply that from the similarity

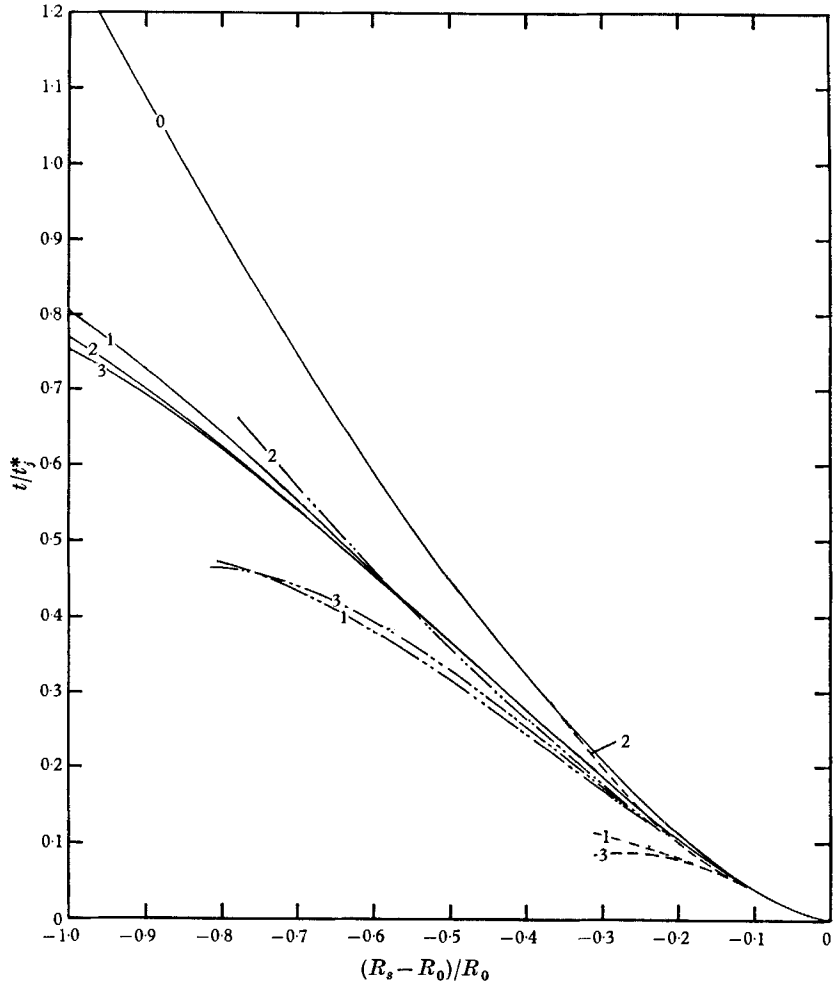

FIGURE 3. Shock trajectories for spherical implosions at different initiation energies. Values of c_j^{*2}: ——, 0; —·—, 0·1; – – –, 0·5. Zeroth-, first-, second- and third-order solutions are shown.

solution where $R_s \sim t^{\frac{2}{3}}$. In the neighbourhood of the wall $x_s = 0$, all the trajectories coincide with the planar one indicating that area contraction effects are small initially. That the collapse is stronger for spherical waves than for the cylindrical waves is clearly illustrated.

The distributions of the particle velocity ϕ and the pressure f behind a collapsing strong spherical shock wave are shown in figures 5 and 6, respectively. The distribution for a strong planar blast wave (which is the zeroth-order solution

in the present analysis) is also plotted at $R_s/R_0 = 0{\cdot}1$ and $0{\cdot}7$ to indicate the effect of area convergence. All the particle velocity profiles decrease monotonically from its value of $0{\cdot}8333$ at the shock front to a constant value at the wall.

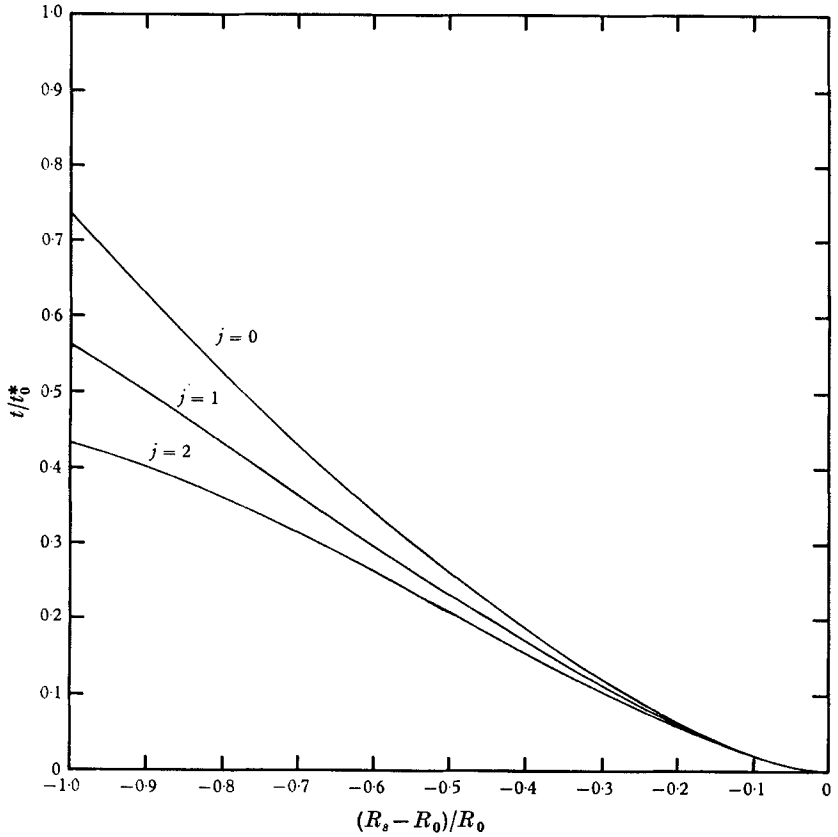

FIGURE 4. Comparison of shock trajectories for strong planar, $j = 0$, cylindrical, $j = 1$, and spherical implosions, $j = 2$, $(c_j^{*2} = 0)$.

The additional adiabatic compression of the shocked states due to area convergence as the shock collapses towards the centre is illustrated by the build-up of pressure in the flow behind the front. A more pronounced indication of this adiabatic compression of the flow can be seen from the density distributions shown in figure 7. Towards the end of the collapse, one notes that the density increases further behind the shock front to a value greater than six times the initial density that is obtained across a strong shock in a perfect gas with $\gamma = 1{\cdot}4$. For the cylindrical case, flow compression due to area convergence is less intense. One notes from the density profiles for strong cylindrical implosion shown in figure 8 that the density peak is not observed until the shock wave is very close to the centre of collapse—the region where the present perturbation solution becomes inaccurate. The further increase in pressure and density behind the shock near the centre of collapse is in qualitative agreement with the similarity solution of Guderley (1942), Butler (1954) and Lee (1966).

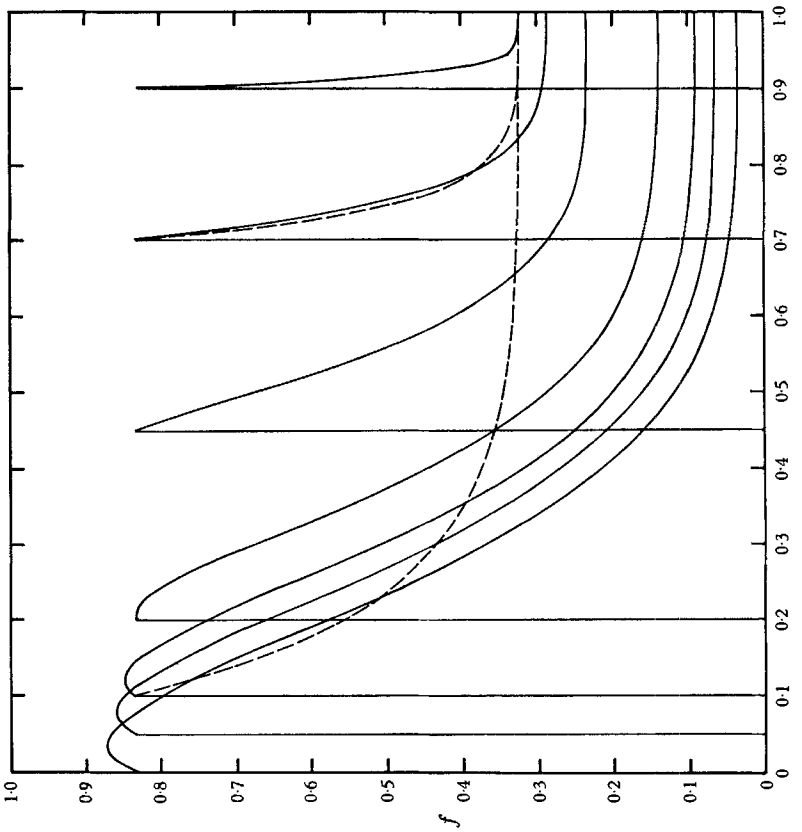

FIGURE 6. Normalized pressure profiles for strong ($c_j^{*2} = 0$), spherical, implosions. - - -, zero order; ——, third order.

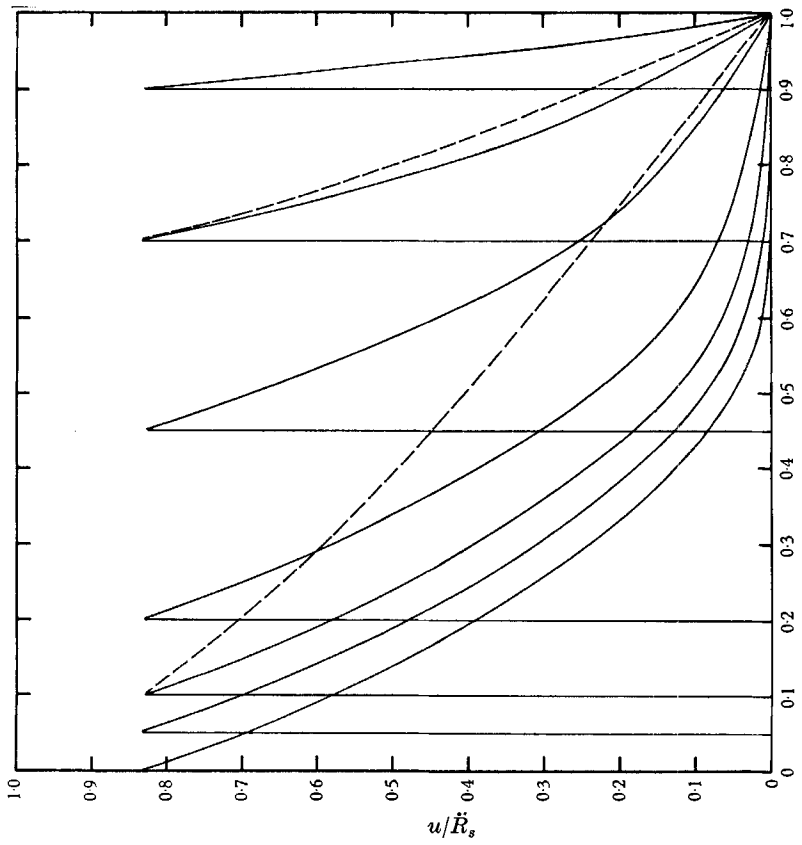

FIGURE 5. Normalized particle velocity profiles for strong ($c_j^{*2} = 0$), spherical, imploding shocks. - - -, zero order; ——, third order.

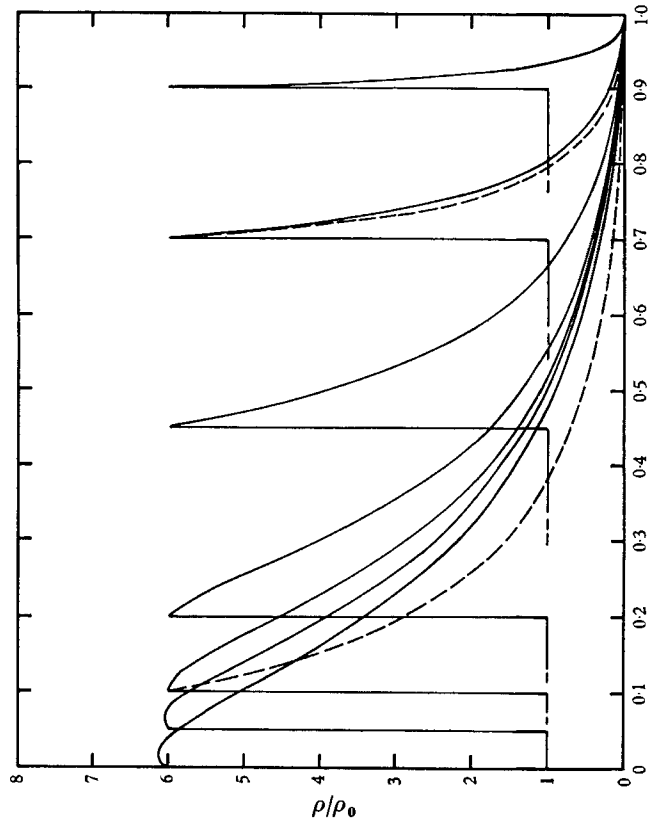

FIGURE 8. Normalized density profiles for strong ($c_j^{*2} = 0$), cylindrical implosions. – – –, zero order; ——, third order.

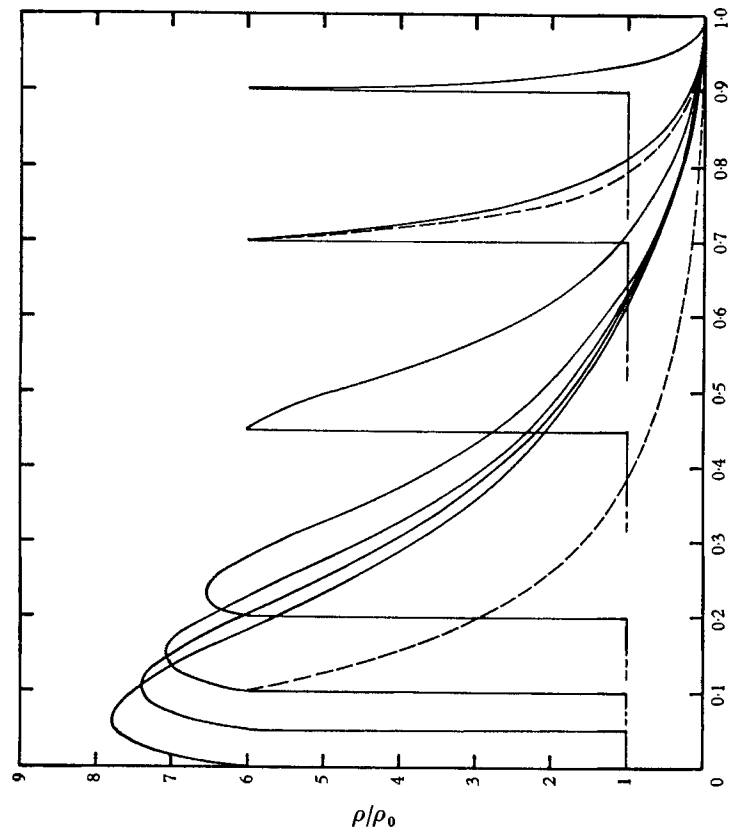

FIGURE 7. Normalized density profiles for strong ($c_j^{*2} = 0$), spherical implosions. – – –, zero order; —— third order.

5. Conclusions

The present analysis provides a fairly accurate and complete description of the initial phases of collapse of impulsively generated implosions. For strong collapse where the initiation blast energy is large (i.e. $c_j^{*2} \to 0$), the present perturbation scheme is simply a Taylor series expansion about the chamber wall $x_s = 0$, and the radius of convergence covers a significant portion of the total collapse. Counter-pressure effects become dominant for weak initiation, and the validity of the present second-order solution is confined to the neighbourhood of the wall whereby $|x_s| \ll 1$. A description of the complete collapse requires a numerical integration scheme. However, the present analysis provides an excellent method for determining the appropriate starting conditions for the numerical solution. The present solution is directly applicable to steady internal axisymmetrical hypersonic flow in a straight cylindrical duct. The perturbation scheme used has been extended to other methods of initiation of the shock wave such as by a collapsing piston which will be analogous to other hypersonic inlet geometries.

This work was supported by the National Research Council of Canada under Grant No. A-3349 and No. A-118 and AFOSR 1290-67. It was first reported at the Canadian Congress of Applied Mechanics, Laval University, Quebec, May 1967.

REFERENCES

BRODE, H. 1955 *J. Appl. Phys.* **26**, 766.

BUTLER, D. S. 1954 *ARE Rep.* no. 54/54.

CHESTER, W. 1954 *Phil. Mag.* **45**, 1293.

CHISNELL, R. F. 1955 *Proc. Roy. Soc.* A **232**, 350.

DENNEN R. S. & WILSON, L. N. 1962 *Exploding Wirs*, vol. 2 (edited by Chace & Moore). New York: Plenum Press.

GLASS, I. I. 1965 *UTIAS Rev.* no. 25.

GUDERLEY, G. 1942 *Luftfahrtforschung*, **19**, 302.

KNYSTAUTAS, R., LEE, B. H. K. & LEE, J. H. 1967 Paper presented at the *6th International Shock Tube Symposium*, Freiburg, Germany. (To appear in the *Phys. Fluids*.)

LEE, B. H. K. 1966 Ph.D. Thesis. McGill University.

LEE, J. H. & LEE, B. H. K. 1965 *Phys. Fluids*, **8**, 2148.

PAYNE, R. B. 1957 *J. Fluid Mech.* **2**, 185.

RAE, W. J. & KIRCHNER, H. P. 1963 *Cornell Aero. Lab. Rep.* no. RM-1655-M-4, N63-16887.

SAKURAI, A. 1954 *J. Phys. Soc. Japan*, **9**, 256.

STANYUKOVICH, K. P. 1960 *Unsteady Motion of Continuous Media* (trans.). Oxford: Pergamon.

WELSH, R. L. 1966 *University of California, Berkeley, Rep.* no. AS-66-1.

WHITHAM, G. B. 1958 *J. Fluid Mech.* **4**, 337.